ACS OMEGA

http://pubs.acs.org/journal/acsodf

Article

# All-Polymer Microcavities for the Fluorescence Radiative Rate Modification of a Diketopyrrolopyrrole Derivative

Heba Megahd, Paola Lova, Samim Sardar, Cosimo D'Andrea, Andrea Lanfranchi, Beata Koszarna, Maddalena Patrini, Daniel T. Gryko, and Davide Comoretto*

Cite This: *ACS Omega* 2022, 7, 15499−15506

Read Online

ACCESS | Metrics & More | Article Recommendations | Supporting Information

**ABSTRACT:** Controlling the radiative rate of emitters with macromolecular photonic structures promises flexible devices with enhanced performances that are easy to scale up. For instance, radiative rate enhancement empowers low-threshold lasers, while rate suppression affects recombination in photovoltaic and photochemical processes. However, claims of the Purcell effect with polymer structures are controversial, as the low dielectric contrast typical of suitable polymers is commonly not enough to provide the necessary confinement. Here we show all-polymer planar microcavities with photonic band gaps tuned to the photoluminescence of a diketopyrrolopyrrole derivative, which allows a change in the fluorescence lifetime. Radiative and nonradiative rates were disentangled systematically by measuring the external quantum efficiencies and comparing the planar microcavities with a series of references designed to exclude any extrinsic effects. For the first time, this analysis shows unambiguously the dye radiative emission rate variations obtained with macromolecular dielectric mirrors. When different waveguides, chemical environments, and effective refractive index effects in the structure were accounted for, the change in the radiative lifetime was assigned to the Purcell effect. This was possible through the exploitation of photonic structures made of polyvinylcarbazole as a high-index material and the perfluorinated Aquivion as a low-index one, which produced the largest dielectric contrast ever obtained in planar polymer cavities. This characteristic induces the high confinement of the radiation electric field within the cavity layer, causing a record intensity enhancement and steering the radiative rate. Current limits and requirements to achieve the full control of radiative rates with polymer planar microcavities are also addressed.

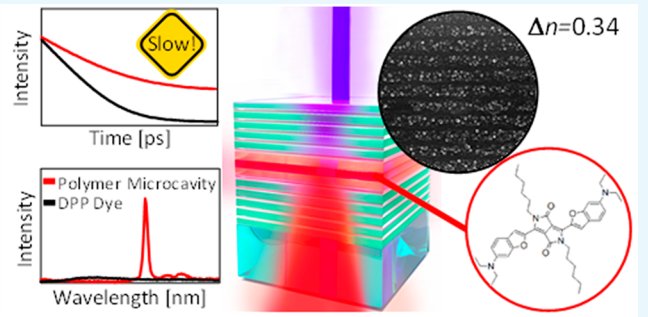


## INTRODUCTION

Progress in the field of polymer photonics has quickly accelerated in the last decades due to their unique properties, including easy chemical tailoring, mechanical flexibility, and simple fabrication.[1] Devices employing all-polymer planar 1D photonic crystals such as light-emitting diodes (LEDs), photovoltaic cells, and sensors[2] are especially appealing as their fabrication is easy to scale up.[3] However, the poor refractive index ($n$) contrast between transparent polymer materials limits light confinement[3] and hinders the control of spontaneous emission rates, namely the Purcell effect.[4] However, empowering the control of an emitter's radiative rate with polymer photonic crystals promises the easy large-area fabrication of either flexible low-threshold lasers[5] and high-efficiency LEDs[6] when the rate is increased, or photovoltaic and photocatalytic devices where an increase in the exciton lifetime (i.e., a reduction of the radiative rate) leads to a longer diffusion length and a higher device performance.[7]

Both radiative rate enhancement and radiative rate suppression have been well-demonstrated in metallic[8] and inorganic[9] structures. Indeed, the latter have been dominating the photonics playground thanks to their low losses and optimal radiation confinement.[10] Rate control has been achieved by employing inorganic optical resonators[11] and microcavities (MCs) of different typologies,[12] including planar ones,[13] microdisks,[14] micropillars,[15] and photonic crystals.[16] On the other hand, their fabrication requires severe conditions and is time and energy consuming. This aspect has hindered their adaptation for flexible devices, integration with organic and hybrid emitters, and large-area production. As such, achieving rate control with polymer structures would be a milestone for efficient solution-processable flexible photonics. Yet, the unambiguous observation of this effect in polymer structures has been disputed within the scientific community. Some claims of Purcell effect observation were made for hybrid

**Received:** January 9, 2022
**Accepted:** March 22, 2022
**Published:** April 25, 2022

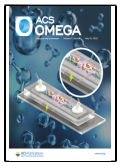

silica/polystyrene systems,[17] but possible extrinsic effects, such as changes in the refractive index of the effective medium,[18] and chemical effects, including exciton chemical traps, impurities, and local disorder affecting the structure, have been debated for these systems.[19] In general, photoluminescence (PL) lifetime ($\tau_{PL}$) variations were reported for polymer synthetic opals[20] and 2D[21] and planar MCs,[22] but radiative rate variations were not investigated. Indeed, $\tau_{PL}$ measurements alone cannot disentangle radiative ($\Gamma_R$) and nonradiative ($\Gamma_{NR}$) decay rates without information on the photoluminescence external quantum efficiency ($\eta$, eq 1).[23] Then, the conclusion that any changes in the fluorescence lifetime arise from a modification of the $\Gamma_R$ value is valid only when $\eta$ is taken into account.

$$\eta = \frac{\Gamma_R}{\Gamma_R + \Gamma_{NR}} \quad (1)$$

In this work, we unambiguously demonstrate radiative rate suppression within a planar polymer MC fabricated through the solution processing of a perfluorinated polymer, Aquivion (AQ, $n$ = 1.35),[2] and polyvinylcarbazole (PVK, $n$ = 1.69).[3,24] The couple provides the highest dielectric contrast demonstrated for polymer planar microcavities ($\Delta n$ = 0.34 in the UV-NIR range) so far.[25] The dye embedded in the cavity is a diketopyrrolopyrrole (DPP) derivative. Diketopyrrolopyrroles are some of the most studied organic dyes for electronics and photonics,[26] including in organic light-emitting diodes and solar cells,[27] due to their tailorable synthesis and high thermal- and photostabilities.[28] The same materials were also employed to fabricate a series of references. A systematic assessment of $\eta$ and the emission decays allows us to unequivocally demonstrate an increase of the radiative lifetime ($\tau_{rad}$) in opportunely tuned microcavities, ruling out any simpler alternative interpretations or extrinsic photophysical processes beside cavity Purcell effects.

## RESULTS

**Cavity Design and Properties.** The MCs were grown via spin-coating deposition and were formed by two dielectric mirrors, each of which consisted of 20 bilayers of AQ and PVK. The cavity between the mirrors contains two layers of cellulose acetate (CA) sandwiching a layer of polystyrene (PS) doped with a DPP derivative[27,29] (DPP:PS), as sketched in Figure 1a. The same panel shows the chemical structure of the DPP dye, while the normalized PL and absorbance spectra of a thin film of the DPP:PS blend cast on a glass substrate are shown in Figure 1b. In the spectral range of interest, the DPP dye shows three distinct absorption maxima at $\lambda$ = 450, 600, and 655 nm (highest intensity). Upon excitation at 534 nm, the steady-state PL spectrum of the blend displays a Stokes shift of 22 nm as the maximum intensity appears at $\lambda$ = 677 nm with a full-width at half-maximum (FWHM) of 40 nm. Additionally, the emission shows a broad shoulder at 745 nm.

The microcavity ($MC_{tuned}$) was engineered to tune the mirrors' photonic band gap (PBG) and cavity mode to the PL of the DPP dye using simple control of the spin-coating deposition parameters. Moreover, several reference samples were engineered and fabricated to compare the properties of the microcavity with those of the bare dye, particularly to exclude radiative rate variations due to extrinsic effects, including medium chemical effects, the polarity of the medium, the residual solvent diffusion among layers, waveguiding, out-

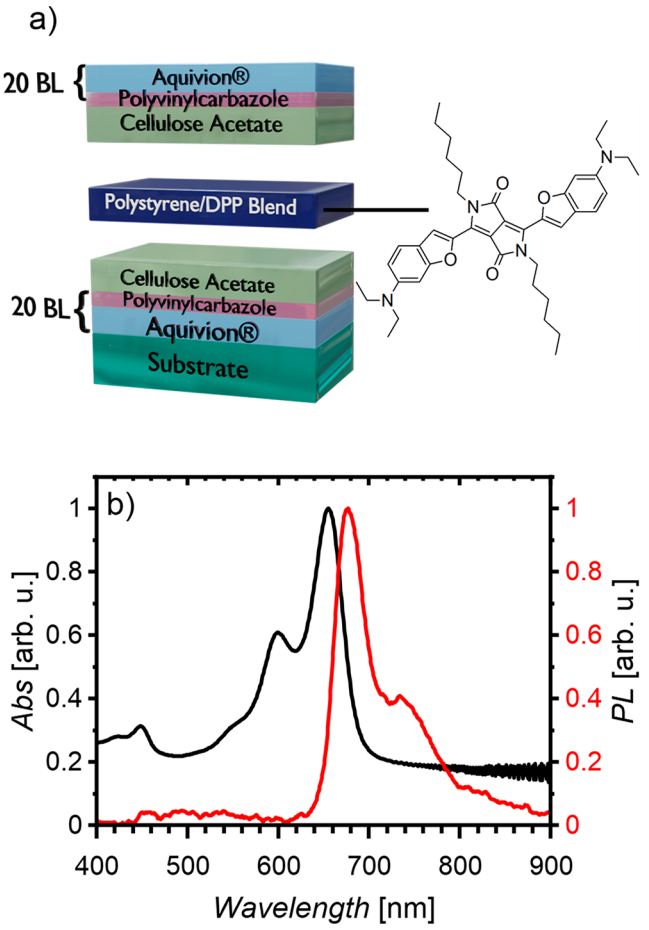


**Figure 1.** (a) Schematic of the MC structure, including the chemical structure of DPP. (b) Normalized absorbance and PL intensity spectra of the DPP:PS blend thin film.

coupling, and light extraction differences.[25] These references were a DPP:PS pristine blend film, a detuned microcavity ($MC_{detuned}$) with the PBG in the green region of the spectrum where the DPP:PS film does not show significant fluorescence, bilayer CA-DPP:PS (R1), and a more complex five-layer structure (R2) (see Supporting Figure S1 for the optical characterization of the thin films). These references serve to simulate possible defects that could be unintentionally inserted into the microcavity by the growth process as well as loss mechanisms such as waveguiding effects and self-absorption, which are known to affect light emission in polymer microcavities.[24]

Figure 2a contrasts the reflectance spectra of both the tuned and detuned microcavities. Both structures display the characteristic features of planar MCs: an intense and wide reflectance band corresponding to the PBG of the photonic crystal mirrors, with a sharp minimum assigned to the cavity mode, and a Fabry−Pérot interference pattern in the background. While the PBG and the cavity mode of $MC_{tuned}$ strongly overlap the emission spectrum of the DPP blend, the shifted microcavity provides no spectral overlap; hence, any variation in the emission of the dye in this sample cannot be assigned to optical confinement effects provided by the microstructure.

For the further characterization of the $MC_{tuned}$, Figure 2b shows the transmittance spectrum of the microcavity, which, corresponding to the reflectance spectrum, shows a wide PBG


https://doi.org/10.1021/acsomega.2c00167
ACS Omega 2022, 7, 15499−15506

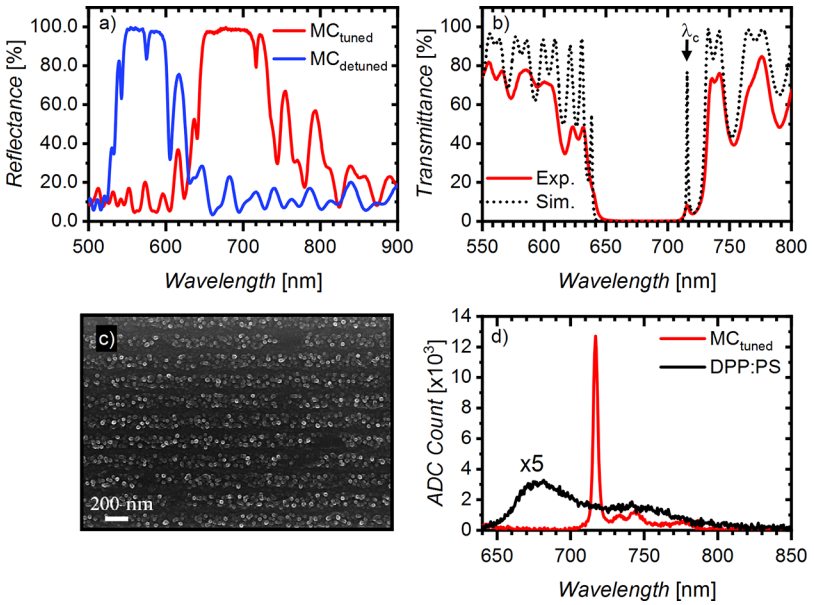


**Figure 2.** (a) Reflectance spectra of tuned microcavity (red line) and the detuned one (blue line). (b) Experimental (red full line) and simulated (black dotted line) transmittance of the tuned microcavity. (c) SEM image of a representative DBR forming the dielectric mirror in a tuned microcavity. (d) Photoluminescence spectra of the DPP:PS film (multiplied by 5, black full line) and the tuned microcavity (red full line).

with a maximum at $\lambda_c$ = 717 nm assigned to the cavity mode. The PBG extends from 635 to 732 nm (FWHM of 250 meV), a larger value compared to other polymer planar microcavities with smaller dielectric contrasts.[25,30] Moreover, due to the photonic band structure of the MC, the spectral position of the aforementioned features is strongly dependent on the angle of incidence and the polarization state of the incoming light beam (Supporting Figure S2),[31] so the emission spectrum can possibly be tuned by changing the detection angle. It is worth noticing that the sample surface shows some minor spectral inhomogeneities due to small thickness variations across the sample, as reported in Supporting Figure S3a. Supporting Figure S3b shows a digital image of the strong PL from a microcavity cast on a flexible substrate under violet laser excitation.

The optical response of the structure was simulated using the complex refractive index dispersions of all the polymers employed that were previously reported in the literature,[2,3,24,32] and that measured for the DPP:PS film (Supporting Figure S4). Employing transfer matrix method (TMM) modeling,[3] the simulated transmittance reported in Figure 2a (dotted line) was best-fit to the experimental one, yielding the thicknesses of individual materials (74.5 nm for PVK, 159.5 nm for AQ, 184 for DPP:PS, and 78 nm for the CA layers).The positions and widths of the interference fringes, as well as the PBG and $\lambda_c$ in the experimental measurements, are all well-reproduced in the calculation. To obtain initial estimates of the layer thicknesses for simulations, SEM measurements were performed, The SEM micrograph in Figure 2c (and Supporting Figure S5) shows the layering of the DBR after the microcavity was freeze-cracked, which caused uneven fracture artifacts in the image. The AQ layers are distinguishable thanks to their spherical aggregates, which have been previously reported in the literature for perfluorosulfonic acid ionomer dispersions.[33] From the SEM images, the uniformity is clear. As described in detail in Supporting Figure S6, the average thickness of the AQ layers was estimated to be 108 ± 8 nm, and that of PVK was estimated to be 65 ± 6 nm. We noticed that the freeze-cracking process induced delamination that prevented the direct observation of the cavity layers, whose thicknesses were then estimated through AFM measurements to be 88 ± 33 nm for the CA layers and 113 ± 67 for the DPP:PS layer (see Supporting Figure S7 for details). We observed good agreement within the experimental uncertainty between thickness derived from SEM/AFM measurements for the PVK, CA, and DPP:PS layers and those derived from optical simulations, while some discrepancy was observed for the AQ layers. However, this is expected as AQ, being a material sensitive to its chemical environment, is strongly perturbated by the abrupt change induced by the freeze-cracking process and the subsequent vacuum environment of the SEM chamber.[2]

Figure 2d compares the PL spectra for a DPP:PS thin film and MC$_{tuned}$. Both the DPP:PS layer in the microcavity and that in the reference DPP:PS film were cast under identical conditions. Due to the spectral overlap of the dye PL with the PBG and the very sharp cavity mode (FWHM of ∼3.5 nm), the local photonic density of states (LPDOS) strongly modulates the fluorescence line-shape.[3,34] Indeed, the LPDOS is very low at the PBG and is strongly enhanced at the cavity mode, channeling the emission into the latter. At near-normal incidence, the enhanced LPDOS at the cavity mode produces a 40-fold intensity enhancement of the DPP emission at $\lambda_c$ = 717 nm as compared to the bare emitter film (see Supporting Figure S8 for a comparison with other spectral regions), a record value among polymer microcavities (the highest being 8.9× to the best of our knowledge).[22b] As the collection angle increases, the PBG and $\lambda_c$ shift to shorter wavelengths, changing the spectral regions that are either enhanced or suppressed (see Supporting Figures S9 and S10 for details). The finesse of MC$_{tuned}$ is quantified through the quality factor ($Q = \lambda_C / \Delta\lambda_C$) of approximately 205, a relatively high value compared to the highest reported so far for all-polymer microcavities ($Q$ = 255).[30] We also notice three additional weak emission peaks at approximately 733, 743, and 775 nm in the cavity PL spectra that corresponded to the local


https://doi.org/10.1021/acsomega.2c00167
ACS Omega 2022, 7, 15499−15506

minima in the Fabry–Pérot interference pattern (Figure 2a). Unsurprisingly, the PL is strongly suppressed at the PBG wavelengths where the LPDOS is lower. As expected from the angular dispersion of transmittance in the microcavities[34] (Supporting Figure S2), the fluorescence from $MC_{tuned}$ is highly directional compared to the Lambertian emission of the DPP:PS film (Supporting Figure S9).

Moreover, we consider the overall microcavity effect on the fluorescence intensity, where only part of the dye's fluorescence spectrum overlaps the PBG and the microcavity mode. Supporting Figure S10 displays the angle-resolved PL intensity data at the cavity mode wavelength as well as those integrated for all wavelengths for the microcavity, the standalone DPP:PS film, and the reference R2. Then the total emission enhancement factor ($G_{tot}^{exp}$) according to eq 2[35] can be calculated as ∼1.4 with respect to the dye and ∼1.3 with respect to R2, indicating an overall enhancement in the PL intensity. The relevant calculations are more thoroughly discussed in the Supporting Information.

$$G_{tot}^{exp} = \frac{\iint PL_{cav}(\lambda, \theta)d\lambda d\theta}{\iint PL_{ref}(\lambda, \theta)d\lambda d\theta} \quad (2)$$

**Cavity Effects and Radiative Rate Modification.** Figure 3 compares the fluorescence decay upon excitation with a pulsed laser ($\lambda$ = 405 nm) for the standalone DPP:PS film (black squares), $MC_{detuned}$ (blue squares), and $MC_{tuned}$ (red squares), which was evaluated from the PL intensity at $\lambda_{MCtuned}$ ± 10 nm. As the reference intensities are lower than the tuned microcavity due to the previously discussed enhancement effect (see Figure 2c), their decay signals have a lower signal-to-noise ratio. Notwithstanding, a strong difference between the lifetimes of $MC_{tuned}$ and the two references can clearly be observed, even without the need for fitting.

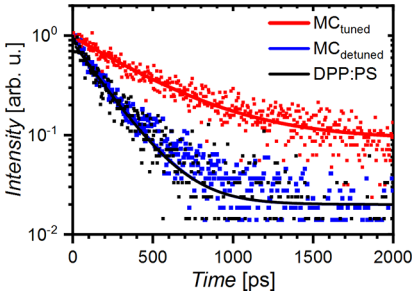


**Figure 3.** Photoluminescence decay (squares) and fitted data (lines) for the tuned microcavity (red) and for two references: the DPP:PS film (black) and a detuned microcavity (blue, $MC_{detuned}$) around $\lambda_c$.

$\tau_{PL}$, which is related to the radiative and nonradiative decay rates $\left(\frac{1}{\tau_{PL}} = \Gamma_R + \Gamma_{NR} = \frac{1}{\tau_R} + \frac{1}{\tau_{NR}}\right)$, was retrieved from the single-exponential fitting of the decays (Figure 3, Supporting Figure S11, and Table S1). Then, the radiative lifetimes for all the samples ($\tau_{rad}$) were calculated as the ratio between the best-fitted $\tau_{PL}$ and the quantum efficiency $\eta$ measured for all samples (Table S1). We would like to stress the role of the external quantum efficiency (eq 1) in disentangling the radiative and nonradiative ($\tau_{NR}$) lifetimes and quantifying the Purcell effect. As reported in eq 3, the radiative rate can only be calculated from the quantum efficiency and the overall PL lifetime. Unfortunately, $\eta$ measurements are rarely reported, making estimations of the actual radiative rate and its variations is highly speculative.[36]

$$\tau_R = \frac{\tau_{PL}}{\eta} \quad (3)$$

The fits for the references are almost superimposable, as seen in Figure 3. The results of such calculations are summarized in Table 1, showing that the two references have similar $\tau_{PL}$ values (190 ps for the DPP:PS layer and 185 ps for $MC_{detuned}$). Comparable lifetimes were also observed for other references that emulated the boundaries of the defect layer (as reported in Table S1 of the Supporting Information), while the value more than doubles (∼416 ps) for the tuned microcavity. Regarding $\eta$ instead, the value for the bare DPP:PS film is ∼6%, which decreases by half for the $MC_{detuned}$ reference (∼3%) and to a sixth for $MC_{tuned}$ (∼1%). Astonishingly, with respect to the DPP:PS film ($\tau_{rad}$ = 3.2 ns), the microcavity shows a 10-fold increase in the radiative lifetime ($\tau_{rad}$ ∼ 42 ns) as compared to a slight increase of that for $MC_{detuned}$ ($\tau_{rad}$ = 6.2 ns). Corresponding changes in the radiative rates were derived $\left(\Gamma_{rad} = \frac{1}{\tau_{rad}}\right)$ and are reported in Table 1.

From data in Table 1, we derived the ratio between the radiative decay rate of the emitter modified by the environment ($\Gamma_{rad}^{mod}$) and its decay in vacuum $\Gamma_{rad}$ ($P$), usually called the Purcell factor. In our case, the average value $P$ = 0.08 (0.03 ≤ $P$ ≤ 0.24, accounting for error) is achieved when considering the DPP:PS film as a reference, and $P$ = 0.15 (0.06 ≤ $P$ ≤ 0.47) considering instead the detuned microcavity as a reference. The latter accounts for enhanced self-absorption due to the small Stokes shift, the longer photon dwell time in the cavity, out-coupling effects, and any variations due to chemical effects or the effective dielectric environment. Notwithstanding the significant error propagating from uncertainty in the quantum yield measurements, the present $P$ values are consistent with strong radiative rate suppression. If, however, the overall PL rates were considered only, i.e., neglecting $\eta$ as often occurs,[23] $P$ would have much larger values (0.44–0.46), falsely indicating a smaller and speculative rate suppression. The PL decay and $\eta$ for all other references used (Table S1) show very similar values to those for references reported in Table 1. Finally, we notice that the effective refractive indices of all our

**Table 1. Radiative Decays: Photoluminescence Lifetime $\tau_{PL}$, Quantum Efficiency $\eta$, and the Calculated Radiative $\tau_{rad}$ and Non-Radiative $\tau_{NR}$ Lifetimes for the Microcavities and the DPP:PS Film[a]**

| sample | $\tau_{PL}$ [ps] | $\eta$ [%] | $\tau_{rad}$ [ns] | $\tau_{NR}$ [ps] | $\Gamma_{rad}$ [ns$^{-1}$] | $\Gamma_{NR}$ [ns$^{-1}$] |
|---|---|---|---|---|---|---|
| DPP:PS | 190 ± 20 | 6 ± 2 | 3.2 ± 1.4 | 202 ± 89 | 0.32 | 4.9 |
| $MC_{detuned}$ | 185 ± 20 | 3 ± 1 | 6.2 ± 2.7 | 191 ± 84 | 0.16 | 5.2 |
| $MC_{tuned}$ | 416 ± 20 | 1 ± 0.5 | 41.6 ± 22.8 | 420 ± 230 | 0.02 | 2.4 |

[a]See Table S1 for more details.



https://doi.org/10.1021/acsomega.2c00167
ACS Omega 2022, 7, 15499−15506

references (also reported in Table S1) show a variation below 10%.

## DISCUSSION

To date, this is the first case where the Purcell effect is unambiguously confirmed in all-polymer planar microcavities. It is then useful to provide a deeper investigation of the phenomena behind it and explain the reasons that prevented its observation so far.

The puzzling results summarized in Table 1 concern the simultaneous reduction in $\eta$ and the increase in $\tau_{PL}$ for the tuned microcavity with respect to all references in both Table 1 and Table S1. Indeed, in contrast with our data (Table 1) where $\Gamma_{NR}$ is almost halved, a decrease in $\eta$ usually causes a decrease in $\tau_{PL}$ due to enhanced nonradiative recombination rates.[37] Moreover, the radiative rate is known to be strongly dependent on the effective refractive index surrounding the emitters, as demonstrated in planar silicon slot waveguides.[19d] The variations in the value of $\tau_{rad}$ between the tuned cavity and the references show remarkable dissimilarity and do not comply with this interpretation because the references have effective refractive indices similar (within 10%, see Table S1) to that of $MC_{tuned}$, making this alternative explanation unsuitable for the radiative rate change observed for our plastic microcavities.

To explain the significant extension of the radiative rate for the $MC_{tuned}$, we must invoke an unusual change in the light−matter interaction: the Purcell-effect, i.e., the modification of the spontaneous emission rate of a quantum system. According to theory, both radiative rate suppression and radiative rate enhancement should be observable in planar microcavities.[13,38] Ideally, rate enhancement is achieved when three conditions are satisfied: (i) the electromagnetic field is strongly confined, (ii) the emission intensity is spectrally sharper than the cavity mode and tuned to the region where the LPDOS is at a maximum, and (iii) the emitter is placed at an antinode of the microcavity electric field standing wave where its intensity is at a maximum. Conversely, if one or more of these conditions is not satisfied, rate suppression should occur.[39]

To discuss the role of these three requirements, it is useful to recall the relevant theoretical framework. According to the Wigner−Weisskopf approximation,[40] the modified emission rate is directly proportional to the LPDOS,[31,41] which is a function of the angular frequency ($\omega$) and of the emitter position ($r$) in the microcavity as described by a modification of Fermi's golden rule $\left(\Gamma_{rad}^{mod} = \frac{2\pi}{\hbar^2}\text{LPDOS}(\omega, \mathbf{r})\right)$.[34] Then, when LPDOS is at a minimum at the band gap, the radiative rate is suppressed, while at the cavity mode (where it is maximum) the radiative rate can be enhanced. Furthermore, if the emitter is placed at an antinode of the electric field amplitude inside the cavity, the emission is enhanced, and vice versa for the positioning at a node. As DPP is a broad-spectrum emitter, all off-resonance photons are expected to experience suppression due to the low density of states outside the cavity mode. This again is assigned to the enhanced dielectric contrast, which is comparable to that achieved in some inorganic dielectric microcavities that exhibited a PL rate enhancement.[38]

Thus far, the achieved result is promising for applications where the suppression of radiative rate and the enhancement of the lifetime are desired effects, such as light-harvesting devices, where the efficiency of the devices is limited by the diffusion length of the excitons and thus by the radiative lifetime.[7] On the other hand, radiative rate enhancement is desired for all light-emission applications, most importantly low-threshold lasers.

Theoretically, the maximum achievable Purcell factor in a cavity ($P_{max}$, eq 4)[10] is dictated by the quality factor $Q$ and the effective cavity volume ($V_{eff}$), which represents the electromagnetic field confinement in all the directions.

$$P_{max} = \frac{3}{4\pi^2}\left(\frac{\lambda}{n}\right)^3 \frac{Q}{V_{eff}} \geq \frac{\Gamma_{rad}^{mod}}{\Gamma_{rad}} \quad (4)$$

In our case, there is no lateral confinement in the plane of the cavity layer. However, we can estimate the relative confinement along the periodicity direction from the penetration depth ($L_{eff}$) of the electromagnetic field into the dielectric mirrors (eq 5). The penetration depth depends on the dielectric contrast ($\Delta n = n_H - n_L$), the geometric length of the defect layers ($L_{MC}$), the optical lengths within the dielectric mirrors ($L_{DBR}$), the periodicity of the structure ($D$), and the effective refractive index ($n_{eff}$).[25]

$$L_{eff} = L_{MC} + 2L_{DBR} = L_{MC} + 4D\frac{n_{eff}}{|n_H - n_L|} \quad (5)$$

In the $MC_{tuned}$ case, $L_{eff}$ is approximately 4.6 $\mu$m, which is much smaller than the overall geometrical length of 9.7 $\mu$m. Then, the system shows a stronger confinement with respect to the previously investigated all-polymer microcavities, where the lower refractive index contrast causes $L_{eff}$ to be comparable or even longer than the photonic structure itself (Table S2). This simple characteristic should explain why radiative rate variations have not been confirmed up to now. In fact, $\Delta n$ = 0.34 represents at least a 50% increase from the highest value reported in the literature for polymer microcavities so far.[22b,42] On the other hand, most of the emission of broad emitters is suppressed by the PBG or is leaked outside the cavity mode, hence indicting the need to integrate very narrow emitters (PL FWHM below the cavity mode width) in the microcavities.

Theoretical and experimental observations indicate that the maximum enhancement or suppression for a narrow emitter placed at the antinode of the standing wave in a planar dielectric microcavity is around 30%.[43] Hybrid planar systems using polymer emitters or spacers in dielectric and metallic systems a report similar enhancement in the overall decay rate, including nonradiative decay.[36,44] However, if micropillars or microbeams with micrometer-scale diameters were fabricated from the planar microcavity, the Purcell factor could reach 10.[45] At the state of the art, lateral nanostructuring remains the most reliable approach to radiative rate enhancement.[10]

From the data reported in Table 1, we noticed that a change in the nonradiative rate was also observed. We suggest here a possible explanation for the effect, even though this is not the main focus of this work. Nonradiative decays are known to be activated after photoexcitation by the photon field.[46] The microcavity deeply changes the environment of the dye and induces the strong localization of the electrical field within the layers driven by the dielectric contrast. In Figure S12, we report the square modulus of the absolute electric field amplitude ($|E|^2$) and its maximum value in the cavity as calculated using TMM;[47] the DPP:PS layer position is highlighted in red. As per the calculations, a strong resonance enhancement of the electric field intensity exceeding 40× the unmodulated intensity can be theoretically expected at a


https://doi.org/10.1021/acsomega.2c00167
ACS Omega 2022, 7, 15499−15506

frequency of the photon field resonant with molecular electronic transitions. According to Siebrand,[46] this enhanced field modifies the Hamiltonian describing the process and thus is a likely explanation for the reduction of the nonradiative rate observed. In agreement with this conclusion, we noticed that no changes of the nonradiative rate were observed for the detuned microcavity, where field enhancement still occurs but is at a frequency nonresonant with the molecular fluorescence.

## CONCLUSION

In conclusion, we demonstrated radiative rate suppression with a 10-fold radiative lifetime increase and record PL enhancement in fully solution-processed polymer planar microcavities, which could open up new perspectives for flexible devices. The larger dielectric contrast employed for the microcavity growth allowed the unambiguous radiative emission rate variation to be observed for the first time thanks to better confinement within the sample thickness. Nevertheless, smaller mode volume as well as the spatial and spectral optimization of fluorophores are still necessary to achieve radiative rate enhancement. The careful synergy of polymer refractive index engineering, advanced dye synthesis, and solution-fabricated flexible structures provides novel perspectives to polymer photonics.

## METHODS

**Dye Synthesis.** DPP was synthesized following the literature procedure.[29a] The dye shows a fluorescence quantum efficiency of 0.55 in toluene solutions (the solvent used to prepare the cavity layer) and essentially the same values in tetrahydrofuran and dichloromethane.

**Microcavity Fabrication.** All samples were grown via the alternating spin coating of 100 $\mu$L of the polymer solutions on 25 × 25 mm$^2$ glass substrates at 175 rps for the dielectric mirrors and 75 rps for the PS-dye solution. The mirrors with 20 bilayers were cast by alternating the deposition of the Aquivion D79-25BS water/ethanol dispersion and the PVK solution in toluene (40 mg/mL). The DPP:PS layer was sandwiched between two layers of CA (30 mg/mL in diacetone alcohol). The top layer serves to prevent water percolation during the subsequent Aquivion deposition, and the bottom one instead serves to maintain the symmetry of the structure. The emitter layer was obtained by casting a solution of the dye in PS/toluene ( 1 mg/mL DPP and 30 mg/mL PS).

**Optical Characterization.** Transmittance measurements were performed with a setup consisting of deuterium and tungsten−halogen sources (spectral range of 230−2500 nm) using an AvaSpec-ULS4096CL-EVO CMOS (spectral range of 200−1100 nm and resolution of 1.4 nm) spectrometer. Angle-resolved spectra were recorded using a homemade setup with an angular resolution ≤1°. Steady-state PL measurements were performed by exciting the samples with an Oxxius 405 nm CW laser focused on a 1 mm$^2$ spot. The fluorescence spectra were collected with the same spectrometer. The collection setup allowed the the transmittance and the PL to be measured on the same sample spot.

**SEM Measurements.** SEM measurements were performed using the FE-SEM Zeiss SUPRA 40 VP instrument (Carl Zeiss, Oberkochen, Germany) at an acceleration voltage of 10 kV. The microcavity sample was frozen in liquid nitrogen and fractured to reveal the cross section upon which a thin carbon layer was deposited using a high-vacuum evaporator (Polaron 6700).

**Time-Resolved PL Measurements.** TRPL measurements were carried out using a femtosecond tunable Ti:sapphire laser (Coherent Chameleon Ultra II) and a streak camera detection system. Type I phase-matched second harmonic generation was performed using a $\beta$-barium borate crystal, leading to pulses with central wavelengths of 405 nm and spot diameters of 6−8 $\mu$m at the sample. The emission was collected at 30° from normal incidence and analyzed by a spectrograph (Princeton Instruments Acton SP2300) coupled to a streak camera (Hamamatsu C5680), resulting in a spectral resolution around 1 nm and a temporal resolution of 20 ps.

**Quantum Efficiency.** External PL quantum efficiencies for microcavities and references were measured by the widely utilized method from de Mello et al.[48] using an integrating sphere (Avantes AvaSphere-50) fiber-coupled with a 405 nm LDH-P-C-405 laser and an Avantes AvaSpec-2048 calibrated spectrometer (200−1150 nm resolution). Typical uncertainty in the quantum efficiency measurements for low values (<10%) can be in the range of 30−50%.[49]

**Refractive Index Measurements.** A VASE instrument (J. A. Woollam Co., Lincoln, NE) in the range 250−2500 nm was used for spectroscopic ellipsometry measurements at different incidence angles from 55° to 75° on films on both fused silica and silicon substrates. Varian Cary 6000i spectrometer in the spectral range of 200−1800 nm was used to measure the reflectance and transmittance at normal incidence. Then, the complex refractive index was evaluated using WVASE32 software (J. A. Woollam, ver. 3.774, Lincoln, NE), adopting oscillator models to guarantee a Kramers−Kronig consistency.

## ASSOCIATED CONTENT

### Supporting Information

The Supporting Information is available free of charge at https://pubs.acs.org/doi/10.1021/acsomega.2c00167.

Further optical characterization of reference samples, complex refractive index of the polymer/dye blend, microscopic characterization of the samples, detailed PL behavior of the tuned microcavity and references, further time-resolved PL decay analysis, comparison among microcavities reported in the literature, and the calculated electric field within the tuned microcavity (PDF)

## AUTHOR INFORMATION


### Corresponding Author

**Davide Comoretto** − *Dipartimento di Chimica e Chimica Industriale, Università degli Studi di Genova, 16146 Genova, Italy;* orcid.org/0000-0002-2168-2851; Email: davide.comoretto@unige.it

### Authors

**Heba Megahd** − *Dipartimento di Chimica e Chimica Industriale, Università degli Studi di Genova, 16146 Genova, Italy;* orcid.org/0000-0003-2385-6648

**Paola Lova** − *Dipartimento di Chimica e Chimica Industriale, Università degli Studi di Genova, 16146 Genova, Italy;* orcid.org/0000-0002-5634-6321

**Samim Sardar** − *Center for Nano Science and Technology at PoliMi, Istituto Italiano di Tecnologia, 20133 Milano, Italy;* orcid.org/0000-0003-1783-6974




https://doi.org/10.1021/acsomega.2c00167
ACS Omega 2022, 7, 15499−15506

**Cosimo D'Andrea** − *Center for Nano Science and Technology at PoliMi, Istituto Italiano di Tecnologia, 20133 Milano, Italy; Dipartimento di Fisica, Politecnico di Milano, 20133 Milano, Italy*

**Andrea Lanfranchi** − *Dipartimento di Chimica e Chimica Industriale, Università degli Studi di Genova, 16146 Genova, Italy;* orcid.org/0000-0003-3642-2611

**Beata Koszarna** − *Institute of Organic Chemistry of the Polish Academy of Sciences, 01-224 Warsaw, Poland*

**Maddalena Patrini** − *Dipartimento di Fisica, Università degli Studi di Pavia, 27100 Pavia, Italy*

**Daniel T. Gryko** − *Institute of Organic Chemistry of the Polish Academy of Sciences, 01-224 Warsaw, Poland;* orcid.org/0000-0002-2146-1282

Complete contact information is available at: https://pubs.acs.org/10.1021/acsomega.2c00167

### Author Contributions

The manuscript was written through contributions of all authors. All authors have given approval to the final version of the manuscript.

### Funding

Work in Genoa was partially supported by the University of Genova (FRA 2019−2020) and by the Ministry of the Instruction, University and Research, through PRIN2020 (2020TS9LXS). Work in Warsaw was financially supported by the Foundation for Polish Science (TEAM POIR.04.04.00-00-3CF4/16-00).

### Notes

The authors declare no competing financial interest.

## ■ ACKNOWLEDGMENTS

We kindly acknowledge Solvay Specialty Polymers for providing us Aquivion and Omar Soda for performing the SEM measurements. Helpful discussion with Prof. G. Lanzani is gratefully acknowledged.

## ■ REFERENCES

(1) Annadhasan, M.; Basak, S.; Chandrasekhar, N.; Chandrasekar, R. Next-Generation Organic Photonics: The Emergence of Flexible Crystal Optical Waveguides. *Adv. Opt. Mater.* **2020**, *8* (21), 2000959.

(2) Megahd, H.; Oldani, C.; Radice, S.; Lanfranchi, A.; Patrini, M.; Lova, P.; Comoretto, D. Aquivion−Poly(N-vinylcarbazole) Holistic Flory−Huggins Photonic Vapor Sensors. *Adv. Opt. Mater.* **2021**, *9* (5), 2170017.

(3) Lova, P.; Manfredi, G.; Comoretto, D. Advances in functional solution processed planar one-dimensional photonic crystals. *Adv. Opt. Mater.* **2018**, *6* (24), 1800730−26.

(4) Purcell, E. M.; Torrey, H. C.; Pound, R. V. Resonance Absorption by Nuclear Magnetic Moments in a Solid. *Phys. Rev.* **1946**, *69* (1−2), 37−38.

(5) Prieto, I.; Llorens, J. M.; Muñoz-Camúñez, L. E.; Taboada, A. G.; Canet-Ferrer, J.; Ripalda, J. M.; Robles, C.; Muñoz-Matutano, G.; Martínez-Pastor, J. P.; Postigo, P. A. Near thresholdless laser operation at room temperature. *Optica* **2015**, *2* (1), 66−69.

(6) (a) Shambat, G.; Ellis, B.; Majumdar, A.; Petykiewicz, J.; Mayer, M. A.; Sarmiento, T.; Harris, J.; Haller, E. E.; Vučković, J. Ultrafast direct modulation of a single-mode photonic crystal nanocavity light-emitting diode. *Nat. Commun.* **2011**, *2*, 539. (b) Cho, H.; Chung, J.; Song, J.; Lee, J.; Lee, H.; Lee, J.; Moon, J.; Yoo, S.; Cho, N. S. Importance of Purcell factor for optimizing structure of organic light-emitting diodes. *Opt. Express* **2019**, *27* (8), 11057−11068.

(7) Vuong, L. T.; Kozyreff, G.; Betancur, R.; Martorell, J. Cavity-controlled radiative recombination of excitons in thin-film solar cells. *Appl. Phys. Lett.* **2009**, *95* (23), 233106.

(8) Murataj, I.; Channab, M.; Cara, E.; Pirri, C. F.; Boarino, L.; Angelini, A.; Ferrarese Lupi, F. Hyperbolic Metamaterials via Hierarchical Block Copolymer Nanostructures. *Adv. Opt. Mater.* **2021**, *9* (7), 2001933.

(9) Gevaux, D. G.; Bennett, A. J.; Stevenson, R. M.; Shields, A. J.; Atkinson, P.; Griffiths, J.; Anderson, D.; Jones, G. A. C.; Ritchie, D. A. Enhancement and suppression of spontaneous emission by temperature tuning InAs quantum dots to photonic crystal cavities. *Appl. Phys. Lett.* **2006**, *88* (13), 131101.

(10) Vahala, K. J. Optical microcavities. *Nature* **2003**, *424* (6950), 839−846.

(11) Jacob, Z.; Smolyaninov, I. I.; Narimanov, E. E. Broadband Purcell effect: Radiative decay engineering with metamaterials. *Appl. Phys. Lett.* **2012**, *100* (18), 181105.

(12) Megahd, H.; Comoretto, D.; Lova, P. Planar microcavities: Materials and processing for light control. *Optical Materials: X* **2022**, *13*, 100130.

(13) Vredenberg, A. M.; Hunt, N. E. J.; Schubert, E. F.; Jacobson, D. C.; Poate, J. M.; Zydzik, G. J. Controlled atomic spontaneous emission from Er3+ in a transparent Si/SiO2 microcavity. *Phys. Rev. Lett.* **1993**, *71* (4), 517−520.

(14) Xie, Z. G.; Götzinger, S.; Fang, W.; Cao, H.; Solomon, G. S. Influence of a Single Quantum Dot State on the Characteristics of a Microdisk Laser. *Phys. Rev. Lett.* **2007**, *98* (11), 117401.

(15) Ding, X.; He, Y.; Duan, Z. C.; Gregersen, N.; Chen, M. C.; Unsleber, S.; Maier, S.; Schneider, C.; Kamp, M.; Höfling, S.; Lu, C.-Y.; Pan, J.-W. On-Demand Single Photons with High Extraction Efficiency and Near-Unity Indistinguishability from a Resonantly Driven Quantum Dot in a Micropillar. *Phys. Rev. Lett.* **2016**, *116* (2), 020401.

(16) Noda, S.; Fujita, M.; Asano, T. Spontaneous-emission control by photonic crystals and nanocavities. *Nat. Photonics* **2007**, *1* (8), 449−458.

(17) (a) Rout, D.; Kumar, G.; Vijaya, R. Amplified emission and modified spectral features in an opal hetero-structure mediated by passive defect mode localization. *J. Phys. D: Appl. Phys.* **2018**, *51* (1), 015112. (b) Petrov, E. P.; Bogomolov, V. N.; Kalosha, I. I.; Gaponenko, S. V. Spontaneous Emission of Organic Molecules Embedded in a Photonic Crystal. *Phys. Rev. Lett.* **1998**, *81* (1), 77−80.

(18) Zhu, Y.; Xu, W.; Zhang, H.; Wang, W.; Tong, L.; Xu, S.; Sun, Z.; Song, H. Highly modified spontaneous emissions in YVO4:Eu3+ inverse opal and refractive index sensing application. *Appl. Phys. Lett.* **2012**, *100* (8), 081104.

(19) (a) Megens, M.; Schriemer, H. P.; Lagendijk, A.; Vos, W. L. Comment on "Spontaneous Emission of Organic Molecules Embedded in a Photonic Crystal. *Phys. Rev. Lett.* **1999**, *83* (25), 5401−5401. (b) Wang, W.; Song, H.; Bai, X.; Liu, Q.; Zhu, Y. Modified spontaneous emissions of europium complex in weak PMMA opals. *Phys. Chem. Chem. Phys.* **2011**, *13* (40), 18023−18030. (c) Petrov, E. P.; Bogomolov, V. N.; Kalosha, I. I.; Gaponenko, S. V.; et al. Petrov et al. Reply: *Reply. Phys. Rev. Lett.* **1999**, *83* (25), 5402. (d) Creatore, C.; Andreani, L. C.; Miritello, M.; Lo Savio, R.; Priolo, F. Modification of erbium radiative lifetime in planar silicon slot waveguides. *Appl. Phys. Lett.* **2009**, *94* (10), 103112.

(20) Priya; Schöps, O.; Woggon, U.; Nair, R. V. Inhibited spontaneous emission using gaplike resonance in disordered photonic structures. *Phys. Rev. A* **2018**, *98* (4), 043835.

(21) Gan, X.; Clevenson, H.; Tsai, C.-C.; Li, L.; Englund, D. Nanophotonic filters and integrated networks in flexible 2D polymer photonic crystals. *Sci. Rep.* **2013**, *3*, 2145.

(22) (a) Lova, P.; Olivieri, M.; Surace, A.; Topcu, G.; Emirdag-Eanes, M.; Demir, M. M.; Comoretto, D. Polymeric Planar Microcavities Doped with a Europium Complex. *Crystals* **2020**, *10* (4), 287. (b) Athanasiou, M.; Papagiorgis, P.; Manoli, A.; Bernasconi, C.; Bodnarchuk, M. I.; Kovalenko, M. V.; Itskos, G. Efficient Amplified Spontaneous Emission from Solution-Processed CsPbBr3

Nanocrystal Microcavities under Continuous Wave Excitation. *ACS Photonics* **2021**, *8* (7), 2120−2129.
(23) Pelton, M. Modified spontaneous emission in nanophotonic structures. *Nat. Photonics* **2015**, *9* (7), 427−435.
(24) Lova, P.; Grande, V.; Manfredi, G.; Patrini, M.; Herbst, S.; Würthner, F.; Comoretto, D. All-polymer photonic microcavities doped with perylene bisimide j-aggregates. *Adv. Opt. Mater.* **2017**, *5* (21), 1700523.
(25) Lova, P.; Megahd, H.; Stagnaro, P.; Alloisio, M.; Patrini, M.; Comoretto, D. Strategies for dielectric contrast enhancement in 1D planar polymeric photonic crystals. *Appl. Sci.* **2020**, *10* (12), 4122.
(26) Skonieczny, K.; Papadopoulos, I.; Thiel, D.; Gutkowski, K.; Haines, P.; McCosker, P. M.; Laurent, A. D.; Keller, P. A.; Clark, T.; Jacquemin, D.; Guldi, D. M.; Gryko, D. T. How To Make Nitroaromatic Compounds Glow: Next-Generation Large X-Shaped, Centrosymmetric Diketopyrrolopyrroles. *Angew. Chem., Int. Ed.* **2020**, *59* (37), 16104−16113.
(27) Grzybowski, M.; Gryko, D. T. Diketopyrrolopyrroles: Synthesis, Reactivity, and Optical Properties. *Adv. Opt. Mater.* **2015**, *3* (3), 280−320.
(28) Bao, W. W.; Li, R.; Dai, Z. C.; Tang, J.; Shi, X.; Geng, J. T.; Deng, Z. F.; Hua, J. Diketopyrrolopyrrole (DPP)-Based Materials and Its Applications: A Review. *Front. Chem.* **2020**, *8*, 679.
(29) (a) Purc, A.; Koszarna, B.; Iachina, I.; Friese, D. H.; Tasior, M.; Sobczyk, K.; Pędziński, T.; Brewer, J.; Gryko, D. T. The impact of interplay between electronic and steric effects on the synthesis and the linear and non-linear optical properties of diketopyrrolopyrrole bearing benzofuran moieties. *Organic Chemistry Frontiers* **2017**, *4* (5), 724−736. (b) Hupfer, M. L.; Koszarna, B.; Ghosh, S.; Gryko, D. T.; Presselt, M. Langmuir−Blodgett Films of Diketopyrrolopyrroles with Tunable Amphiphilicity. *Langmuir* **2021**, *37* (34), 10272−10278.
(30) Manfredi, G.; Lova, P.; Di Stasio, F.; Krahne, R.; Comoretto, D. Directional Fluorescence Spectral Narrowing in All-Polymer Microcavities Doped with CdSe/CdS Dot-in-rod Nanocrystals. *ACS Photonics* **2017**, *4* (7), 1761−1769.
(31) *Organic and Hybrid Photonic Crystals*; Comoretto, D., Ed.; Springer International Publishing: Basel, Switzerland, 2015.
(32) Sultanova, N.; Kasarova, S.; Nikolov, I. Dispersion Properties of Optical Polymers. *Acta Phys. Polym., A* **2009**, *116*, 585.
(33) da Silva, J. S.; Carvalho, S. G. M.; da Silva, R. P.; Tavares, A. C.; Schade, U.; Puskar, L.; Fonseca, F. C.; Matos, B. R. SAXS signature of the lamellar ordering of ionic domains of perfluorinated sulfonic-acid ionomers by electric and magnetic field-assisted casting. *Phys. Chem. Chem. Phys.* **2020**, *22* (24), 13764−13779.
(34) Barth, M.; Gruber, A.; Cichos, F. Spectral and angular redistribution of photoluminescence near a photonic stop band. *Phys. Rev. B* **2005**, *72* (8), 085129.
(35) Schubert, E. F.; Hunt, N. E. J.; Micovic, M.; Malik, R. J.; Sivco, D. L.; Cho, A. Y.; Zydzik, G. J. Highly Efficient Light-Emitting Diodes with Microcavities. *Science* **1994**, *265* (5174), 943−945.
(36) Wang, J.; Cao, R.; Da, P.; Wang, Y.; Hu, T.; Wu, L.; Lu, J.; Shen, X.; Xu, F.; Zheng, G.; Chen, Z. Purcell effect in an organic-inorganic halide perovskite semiconductor microcavity system. *Appl. Phys. Lett.* **2016**, *108* (2), 022103.
(37) *Excited States and Photochemistry of Organic Molecules*; Klessinger, M.; Michl, J., Eds.; VCH: New York, NY, 1995.
(38) Goldberg, D.; Menon, V. M. Enhanced amplified spontaneous emission from colloidal quantum dots in all-dielectric monolithic microcavities. *Appl. Phys. Lett.* **2013**, *102* (8), 081119.
(39) (a) Yamamoto, Y.; Machida, S.; Björk, G. Micro-cavity semiconductor lasers with controlled spontaneous emission. *Opt. Quantum Electron.* **1992**, *24* (2), S215−S243. (b) Bjork, G. On the spontaneous lifetime change in an ideal planar microcavity-transition from a mode continuum to quantized modes. *IEEE J. Quantum Electron.* **1994**, *30* (10), 2314−2318. (c) Björk, G.; Machida, S.; Yamamoto, Y.; Igeta, K. Modification of spontaneous emission rate in planar dielectric microcavity structures. *Phys. Rev. A* **1991**, *44* (1), 669−681.
(40) Scully, M. O.; Zubairy, M. S. *Quantum Optics*; Cambridge University Press: Cambridge, U.K., 1997.
(41) Frezza, L.; Patrini, M.; Liscidini, M.; Comoretto, D. Directional enhancement of spontaneous emission in polymer flexible microcavities. *J. Phys. Chem. C* **2011**, *115* (40), 19939−19946.
(42) Menon, V. M.; Luberto, M.; Valappil, N. V.; Chatterjee, S. Lasing from InGaP quantum dots in a spin-coated flexible microcavity. *Opt. Express* **2008**, *16* (24), 19535−19540.
(43) Tanaka, K.; Nakamura, T.; Takamatsu, W.; Yamanishi, M.; Lee, Y.; Ishihara, T. Cavity-Induced Changes of Spontaneous Emission Lifetime in One-Dimensional Semiconductor Microcavities. *Phys. Rev. Lett.* **1995**, *74* (17), 3380−3383.
(44) (a) Chebykin, A. V.; Orlov, A. A.; Shalin, A. S.; Poddubny, A. N.; Belov, P. A. Strong Purcell effect in anisotropic $\epsilon$-near-zero metamaterials. *Phys. Rev. B* **2015**, *91* (20), 205126. (b) Lemmer, U.; Hennig, R.; Guss, W.; Ochse, A.; Pommerehne, J.; Sander, R.; Greiner, A.; Mahrt, R. F.; Bässler, H.; Feldmann, J.; Göbel, E. O. Microcavity effects in a spin-coated polymer two-layer system. *Appl. Phys. Lett.* **1995**, *66* (11), 1301−1303.
(45) Böckler, C.; Reitzenstein, S.; Kistner, C.; Debusmann, R.; Löffler, A.; Kida, T.; Höfling, S.; Forchel, A.; Grenouillet, L.; Claudon, J.; Gérard, J. M. Electrically driven high-Q quantum dot-micropillar cavities. *Appl. Phys. Lett.* **2008**, *92* (9), 091107.
(46) Siebrand, W., Nonradiative Processes in Molecular Systems. In *Dynamics of Molecular Collisions*, Part A; Miller, W. H., Ed.; Springer: Boston, MA, 1976; pp 249−302.
(47) Sukhoivanov, I. A.; Guryev, I. V. *Photonic crystals: Physics and Practical Modeling*; Springer Series in Optical Sciences, Vol. *152*; Springer Verlag: Berlin, Germany, 2009.
(48) de Mello, J. C.; Wittmann, H. F.; Friend, R. H. An improved experimental determination of external photoluminescence quantum efficiency. *Adv. Mater.* **1997**, *9* (3), 230−232.
(49) (a) Theander, M.; Inganäs, O.; Mammo, W.; Olinga, T.; Svensson, M.; Andersson, M. R. Photophysics of Substituted Polythiophenes. *J. Phys. Chem. B* **1999**, *103* (37), 7771−7780. (b) Valenta, J. Determination of absolute quantum yields of luminescing nanomaterials over a broad spectral range: from the integrating sphere theory to the correct methodology. *Nanoscience Methods* **2014**, *3* (1), 11−27.


https://doi.org/10.1021/acsomega.2c00167
*ACS Omega* 2022, 7, 15499−15506